EUROPEAN ORGANIZATION FOR NUCLEAR RESEARCH

CERN-PPE/90-186
14 December 1990

# A SEARCH FOR WEAKLY INTERACTING NEUTRAL PARTICLES IN MISSING ENERGY EVENTS IN 450 GeV/c PN COLLISIONS

T. Åkesson[3], S. Almehed[6], A.L.S. Angelis[20], H. Atherton[3], P. Aubry[8], H.W. Bartels[4], G. Beaudoin[8], J.M. Beaulieu[8], H. Beker[3], O. Benary[18], D. Bettoni[3,a], V. Bisi[19], I. Blevis[3,b], H. Bøggild[3,c], W. Cleland[12], M. Clemen[12], F. Corriveau[7], S. Dagan[18], K. Dederichs[3,d], S. Dell'Uomo[13], P. Depommier[8], N. DiGiacomo[5], S. DiLiberto[13], J.R. Dodd[20], B. Dolgoshein[10], A. Drees[4], H. En'yo[3], B. Erlandsson[17], M.J. Esten[20], C.W. Fabjan[3], P. Fischer[4], A. Gaidot[15], F. Gibrat-Debu[15], P. Giubellino[19], P. Glassel[4], U. Goerlach[3], R. Haglund[6], L.A. Hamel[7], H. van Hecke[5], V. Hedberg[3], R. Heifetz[18], A. Holscher[4], B. Jacak[5], G. Jarlskog[6], S. Johansson[6], H. Kraner[2], V. Kroh[4], F. Lamarche[7], C. Leroy[7], D. Lissauer[2,18], G. London[15], B. Lorstad[6], A. Lounis[8], F. Martelli[19], A. Marzari-Chiesa[19], M. Masera[19], M.A. Mazzoni[3], E. Mazzucato[7], N.A. McCubbin[14], P. McGaughey[5], F. Meddi[13], U. Mjörnmark[6], M.T. Muciaccia[1], S. Muraviev[9], M. Murray[12], M. Neubert[4], P. Nevski[10], S. Nilsson[17], L. Olsen[2], Y. Oren[18], J.P. Pansart[15], Y.M. Park[12], A. Pfeiffer[4], F. Piuz[3], V. Polychronakos[2], V. Pomianowski[12], G. Poulard[3], M. Price[3], D. Rahm[2], L. Ramello[19], L. Riccati[19], G. Romano[16], G. Rosa[13], L. Sandor[3], J. Schukraft[3], M. Sekimoto[3,e], M. Seman[3,f], A. Shmeleva[9], V. Sidorov[11], S. Simone[1], Y. Sirois[7], H. Sletten[3], S. Smirnov[10], W. Sondheim[5], H.J. Specht[4], E. Stern[12], I. Stumer[2], J.W. Sunier[5], V. Tcherniatin[10], J. Thompson[12], V. Tikhomirov[9], G. Vasseur[15], R.J. Veenhof[3,g], R. Wigmans[3], W.J. Willis[3] and P. Yepes[7]

**HELIOS Collaboration**

## Abstract

We have measured the inclusive cross-section as a function of missing energy, due to the production of neutrinos or new weakly interacting neutral particles in 450 GeV/c proton-nucleus collisions, using calorimetric measurements of visible event energy. Upper limits are placed on the production of new particles as a function of their energy. These upper limits are typically an order of magnitude lower than those obtained in previous searches.

(Submitted to Zeitschrift Für Physik C)

1) University of Bari and INFN, I-70100 Bari, Italy
2) Brookhaven National Laboratory, Upton, NY 11973, USA
3) CERN, CH-1211 Geneva 23, Switzerland
4) University of Heidelberg, D-6900 Heidelberg, Fed. Rep. Germany
5) Los Alamos National Laboratory, Los Alamos NM87544, USA
6) University of Lund, S-223 62 Lund, Sweden
7) McGill University, Montreal, PQ H3A 2T8 Canada
8) University of Montreal, Montreal PQ HC3 3J7 Canada
9) Lebedev Institute of Physics, SU-117924 Moscow, USSR
10) Institute of Physics and Engineering, SU-115409 Moscow, USSR
11) Institute of Nuclear Physics, 630 090 Novosibirsk, USSR
12) University of Pittsburgh, Pittsburgh PA 15260, USA
13) University of Rome 'La Sapienza' and INFN, I-00185 Rome, Italy
14) Rutherford Appleton Laboratory, Didcot OX1 OQX, UK
15) DPhPE, CEN–Saclay, F-91191 Gif-sur-Yvette, France
16) University of Salerno and INFN, I-84100 Salerno, Italy
17) University of Stockholm, S-11346, Stockholm, Sweden
18) University of Tel Aviv, Ramat Aviv 9978 Israel
19) University of Turin and INFN, I-10100 Turin, Italy
20) University College London, London WC1E 6BT, UK
Visitor at CERN from:
a) University of Syracuse, Syracuse, NY 13244-1130, USA
b) Weizmann Institute, Rehovot, Israel
c) Niels Bohr Institute, DK-2100 Copenhagen 0, Denmark
d) Ludwig–Maximilians–Universität, D-8000 Munich 40, Fed. Rep. Germany
e) Institute of Nuclear Study, Tokyo 188, Japan
f) Slovak Academy of Sciences, CS-04353 Kosice, Czechoslovakia
g) NIKHEF-H, NL-1009 DB Amsterdam, The Netherlands.

## 1 Introduction

Weakly interacting neutral particles (WINPs) are of particular interest at present since they may reflect the properties of both the Higgs and of a lightest supersymmetric particle, if they exist. In this paper we report on a search for such particles produced in p-nucleus collisions at 450 GeV/c.

Several recent experiments [1] have searched for unstable neutral particles by looking for their decay products in a certain fiducial volume. The production limits so obtained are valid up to some upper value of the particle life-time. In the present analysis, we have looked for evidence of WINP production in 450 GeV/c pN interactions by studying missing energy events in a $4\pi$-coverage calorimeter system. Hence in our case WINPs have to traverse the detector before decaying in order to give a missing energy signature. Therefore our limits are valid from a certain lower life-time value, and of course do not depend on any assumption on the nature of the WINP decay. A similar analysis has been performed in [2], but, in an experiment with an order of magnitude larger statistics, we become sensitive to the neutrinos from charm decay. The uncertainties in this process set the ultimate limit in the sensitivity to new sources of missing energy.

We present results from missing energy data taken in two different and complementary configurations of the same basic experimental set-up: firstly, from proton interactions in a beryllium wire target with $4\pi$ calorimeter coverage and secondly, from proton interactions occurring in the forward calorimeter itself.

The paper is organised as follows. The experimental set-up is presented in Section 2, followed by a description of the data reduction and analysis for the two detector modes in Section 3. The results are presented and discussed in Section 4, and conclusions are given in Section 5.

## 2 Experimental setup

The HELIOS (High-Energy Lepton and IOn Spectrometer) detector is situated in the H8 beam line of the CERN Super Proton Synchrotron (SPS). An overview of the apparatus is shown in Figure 1. The detector elements used in this analysis are described below; first those corresponding to data taking with the beryllium target ("target" mode) and second, the (minor) modifications needed to study proton interactions in the forward calorimeter ("beam dump" mode). For both configurations the data were taken using the 450 GeV/c proton "micro"-beam developed specially for the HELIOS experiment. This beam has excellent momentum resolution ($\delta$p/p = 0.1%) and a transverse diameter of $\sim$ 50 $\mu$m at the target. Since undetected upstream interactions are a potentially serious background, our unusually small and clean beam is a key element in this experiment.

### 2.1 Target mode

Incoming protons are defined by two small scintillator counters placed 150 cm upstream of the target. The target itself is a 50 $\mu$m-diameter beryllium wire, 2 cm in length. Two additional scintillators act as a halo counter and are used to veto interactions upstream of the target.

A silicon detector [3] consisting of an array of 400 silicon pad elements is centred on the beam axis 15 cm downstream of the target, with a central hole to allow non-interacting beam particles to pass through. This device provides the interaction trigger and measures the charged particle multiplicity.

The target is surrounded by an almost hermetic box of calorimeter modules (the

BOX, WALL and MAGCAL in Figure 1), covering polar angles from $\sim 6.3^0$ ($\eta_{lab} = 2.9$) up to $\sim 95.7^0$ ($\eta_{lab}$ = -0.1). The forward region of the box ($2.2 < \eta_{lab} < 2.9$) is occupied by an Fe/scintillator calorimeter of 3.2 interaction lengths ($\lambda_i$) depth. The remainder of the box consists of U/scintillator and U/Cu/scintillator (UCAL) modules, each divided into an electromagnetic section (6.4 radiation lengths deep) and an hadronic section (4.0 and 3.8 $\lambda_i$ for U and U/Cu module respectively). The calibration and analysis of these devices has been described previously [4, 5, 6]. The forward region ($\eta_{lab} > 2.9$), in which most of the energy is deposited, comprises a U/liquid argon calorimeter (ULAC) followed by additional U/scintillator modules (the BEAM and VETO) giving a total of 10.3 $\lambda_i$ sensitive depth along the beam direction. The ULAC is also divided into two sections, an 18 radiation length electromagnetic section with tower readout and a 4.5 $\lambda_i$ hadronic section with interleaved strip readout. The electromagnetic section has a 5 cm-diameter hole around the beam axis so that non-interacting beam particles and very forward secondaries will hit the hadronic section directly. (Such particles would otherwise begin to shower in the electromagnetic section, degrading the information on secondaries produced at slightly wider angles). Full details of the ULAC design and construction have been given in [7].

Both the liquid argon and scintillator calorimeters have two parallel readouts. The first system, using fast analogue and digital summation of the total energy, allows construction of a wide range of calorimeter triggers. For the data used in this analysis, the digital flash ADC (FADC) modules were configured to trigger on the difference between beam and measured calorimeter energies to provide a missing energy ($E_{mis}$) trigger. The FADC system also incorporates an array of sampling "History" ADC (HADC) modules, which provide information on the time evolution (over 1 $\mu$s) of pulses in each element of the calorimetry. Details may be found in [6]. The second readout system is used exclusively for offline analysis and provides information from each individual channel in the calorimeters. For the ULAC, this system is based on peak-sensing ADCs (PADCs); the equivalent readout for the UCALs uses charge-integrating ADCs (QADCs).

Immediately downstream of the calorimeters is a large acceptance ($\sim$ 100 mrad) muon spectrometer (see Figure 1). It consists of 7 proportional chambers with a total of 32 wire planes, a superconducting dipole magnet and two scintillator hodoscopes, separated by an 80 cm iron wall [8]. Energy loss in the calorimeters and the transverse momentum kick from the magnet combine to give a lower momentum threshold of $\sim$ 5 GeV/c for detected muons.

Several triggers were applied for data-taking. The "minimum bias" interaction trigger requires a signal from the beam-defining scintillators and a minimum of three hits in the silicon pad detector. A missing energy trigger requires the interaction trigger in coincidence with a missing energy signal from the calorimeter system. Good statistical coverage over the full missing energy range was achieved by appropriate downscaling of events satisfying the interaction trigger and missing energy triggers with several different calorimeter $E_{mis}$ thresholds. It has been checked in both these and other data that energy triggers from the calorimeter system introduce no significant inefficiency. In addition, events were recorded using a "random" trigger. These events, taken during beam bursts, were used offline to monitor the detector stability.

### 2.2 Beam Dump mode

For the beam dump configuration, the beryllium target was removed and the beam passed through the hole in the electromagnetic section of the ULAC to impinge directly

on the hadronic section. An additional beam scintillator counter was added, and used in coincidence with the existing counters to define valid incoming beam particles.

Data taking was carried out exactly as for the target mode data, except that the interaction trigger was replaced by the valid beam condition.

# 3 Analysis

## 3.1 Target Mode Data

The first step in the analysis is to check for valid detector information for each event. The data are then filtered through the standard HELIOS calorimeter reconstruction software to obtain calibrated energy information. Two cuts are applied to reduce contamination from non-target interactions: firstly, a requirement is made that there be no hits in either of the veto scintillator counters, and secondly, events are required to have less than 15 hits in the silicon pad counter.

Analysis of this type of data requires particular attention to backgrounds. There are several sources which may fake a missing energy signal: upstream interactions, energy leakage from particle punch-through in the calorimeter, instrumental effects due to pile-up of two or more particles, and energy loss through cracks in the detector coverage.

### 3.1.1 Upstream interactions

Upstream interactions may fake a missing energy signal if all of the following conditions are satisfied: some of the produced secondaries are not detected in the calorimeter, and no particle hits the veto counter, but one particle hits the beam scintillators and hits and interacts in the 50 $\mu$m-diameter target. Contamination from upstream interactions satisfying these criteria is estimated to be negligible.

### 3.1.2 Punch-through

Due to the finite length of the calorimeters the probability that a particle traverses them without interacting is not zero. Any charged particle emerging from the back of the last calorimeter (VETO) will give a signal in the chambers of the muon spectrometer. For this reason only events with no hits in those chambers are selected for further analysis. If the particle emerging from the VETO calorimeter is neutral, it will not be detected in the chambers. Nevertheless it will have a high probability of interacting in the iron wall of the muon spectrometer creating a shower that will be detectable in the hodoscope placed behind the wall. Accordingly, events with any hits in the muon hodoscopes are discarded. The contribution from neutral particle punch-through after this cut is estimated to be negligible. A further cut applied to reduce any remaining punch-through improves shower containment in the calorimeters by demanding that the energy in the forward BEAM calorimeter (see Figure 1) be less than 20% of the total visible energy.

It may be noted that this last cut should not discriminate in any way among events with different values of $E_{mis}$, and so does not affect the shape of the true $E_{mis}$ spectrum. We have deliberately used cuts with this property wherever possible.

### 3.1.3 Pile-up

Because of the pulse-shaping performed on the ULAC calorimeter signals, two events close enough in time, but not exactly coincident, may result in a superposition of the bipolar shaped signals which fakes an event with missing energy. Various methods are used to reduce this background. The simplest is to use the beam counters to reject

events with another incoming projectile in a $\pm 1\mu s$ window (the length of the typical bipolar ULAC pulse is $\sim$ 900 ns). However due to counter inefficiencies, a non-negligible background remains and other methods have to be used. In general the overlap of two events close in time is clearly visible in the History ADC (HADC) system, and a simple computer algorithm is used to reject the events. The systematic error introduced by applying this HADC algorithm is estimated to be of the order of 10%, mainly due to HADC inefficiencies. In addition, pile-up events usually produce different energy values in the two calorimeter readout systems (FADC and PADC-QADC) due to the different time response of the two systems. Hence, in addition to the two previous requirements, the signals provided by the two readout systems are required to be equal within fluctuations.

Any pile-up effect will be proportional to the square of the beam rate. In order to verify that the pile-up contamination is negligible after the application of the three cuts just described, the remaining signal is studied as a function of beam rate. No significant dependence on beam rate is found within statistical errors and therefore at our present level of sensitivity the pile-up contribution is negligible.

### 3.1.4 Cracks

Cracks in the calorimeter coverage may also fake missing energy events. The calorimeter coverage for the target mode data consists of several separate calorimeters, as described in Section 2.1. It is instructive to study, for each component calorimeter individually, the correlation between the energy measured in that component calorimeter and the event missing energy. Any crack in or around a component calorimeter will produce a positive correlation between the energy measured in that calorimeter and the event missing energy, since the greater the energy measured in the component the greater will be the leakage through the crack. This correlation was studied for each of the calorimeter components. No correlation was found except for the electromagnetic section of the ULAC which has an insensitive zone around its central hole [7]. On average, 90% of the energy produced in a collision is deposited in the ULAC, and so any crack in the calorimeter coverage in this region will be particularly important. The crack around the ULAC central hole results in a marked excess of events with apparent $E_{mis} \sim 70$ GeV.

To deal with this problem, we define the fraction of energy in the region close to the crack to be $Q = E_a/E_{vis}$, where $E_a$ is the energy detected in the first set of electromagnetic towers around the hole and $E_{vis}$ is the total energy detected in the calorimeters. Figure 2 shows the spectrum of Q in three $E_{mis}$ bins. The first graph (a) corresponds to small $E_{mis}$ where the missing energy faked by the crack is negligible. The full line in the second plot (b) corresponds to the bin where the crack effect is maximum ($E_{mis}$ = 60-80 GeV) as is illustrated by the appearance of a prominent bump centred at around Q = 0.15. This indicates that for this $E_{mis}$ bin, a large fraction of the events have significant energy deposit in the calorimeter towers around the hole, with consequent energy loss in the neighbouring insensitive material.

In order to correct for this crack effect we make the assumption that the energy distribution in phase space should not be strongly dependent on $E_{mis}$. In other words we assume that the Q spectrum shape, due to events with real missing energy, is only weakly dependent on $E_{mis}$. With this assumption the Q spectrum in the lowest $E_{mis}$ bin (reference spectrum (a)), where the crack contribution is negligible, is used, with the appropriate scaling, to estimate the number of events with real missing energy in the different $E_{mis}$ bins. These are represented in Figure 2 (b) and (c) by dashed histograms. The reference

spectrum is scaled to the first bin of the distribution where the crack contribution is estimated to be negligible in all cases. The systematic error introduced in the subtraction is estimated to be up to 30% in the bin $E_{mis}$ = 60-80 GeV where the effect is maximum.

As already stated above, we have deliberately used cuts which do not depend on $E_{mis}$ wherever possible. The trigger requirement of at least 3 hits in the silicon pad counter has been studied by Monte Carlo, and turns out to be a bias favouring large $E_{mis}$. This effect has been corrected for in the final analysis. It is a 30% correction at $E_{mis} \sim 200$ GeV.

The final sample of events is equivalent to $\sim 10^6$ protons interacting in the target.

### 3.2 Beam Dump Data

The sources of background and contamination in the beam dump data are broadly similar to those described above for the target data. However, the techniques used to remove them differ in several important respects, as described below.

#### 3.2.1 Upstream interactions

Upstream interactions are a potential source of background, as in the target mode data. For the beam dump data the veto protection consists of demanding no hits in either of the veto scintillators in the beam line (as was done for the target mode data), and is extended to include the silicon pad detector and all the off-axis calorimetry (namely the backward calorimeters and the electromagnetic section of the ULAC). By requiring no energy deposition in any of these elements, off-axis particles between 0.12 cm and 240 cm from the beam axis are rejected.

#### 3.2.2 Punch-through

The first requirement is that the primary interaction should take place within the first 1.5 $\lambda_i$ of the hadronic section of the calorimeter. This ensures that the most of the depth of the calorimeter is available for shower absorption, thereby reducing the probability of energy leakage via punch-through. The remaining cuts applied to the beam dump data to eliminate energy leakage from punch-through are similar to those used in the target analysis. Events with hits in the spectrometer chambers or hodoscope planes are rejected and the energy in the BEAM calorimeter restricted to be at most 10% of the total visible energy. This is a more restrictive cut than the 20% used in the target analysis due to the increased fraction of energy deposited in the forward calorimetry in the beam dump configuration.

#### 3.2.3 Pile-up

Pile-up of two or more beam particles within the sensitive time window of the calorimeters is also a source of false missing energy events in beam dump mode. Information from the beam counters is again used to veto events in which additional particles are detected within a $\pm 1\mu$s window around the trigger particle. Good correlation between the parallel calorimeter readouts (PADC and FADC) is also required as described in Section 3.1. Event rejection of overlapping pulses using the History ADCs was unfortunately not possible for the beam dump data due to technical difficulties during data-taking, and analysis of the missing energy spectrum as a function of beam rate shows a residual contamination due to pile-up. This can be seen in Figure 3, which shows the fraction of events in four $E_{mis}$ bins as a function of the beam rate squared. For $E_{mis} > 20$ GeV the data

are compatible with the expected linear dependence on the squared beam rate, and an extrapolation is made to zero beam flux to obtain the rate-independent spectrum. This extrapolation implies at most a 10% correction.

The final data sample in beam dump configuration is equivalent to approximately 3 x $10^7$ interactions, taken at an average beam rate of 4 x $10^4$ protons/s.

## 4 Results

The missing energy spectra, expressed as probability per event, for the target and beam dump data are shown in Figure 4. All cuts and corrections have been applied. The error bars represent combined statistical and systematic errors added in quadrature. The dashed curves are Gaussian distributions with $\sigma = 15$ and $\sigma = 11$ GeV, reflecting the calorimeter resolution for target and beam dump configurations respectively. In both cases, the data points follow the Gaussian up to about $4\sigma$ deviation from average beam energy. The data also show a tail of events extending well beyond the expected calorimeter resolution to missing energies of 200 GeV or more. The results from the two configurations are in very good agreement. Since the target nucleus is beryllium for the target mode data and effectively uranium for the beam dump mode, the agreement between the two data sets implies that the $A$ dependence of the missing energy tail is similar to that of the inelastic cross-section. Parametrising the $A$ dependence of the $E_{mis} > 80$ GeV tail as $A^{\alpha+\delta}$, where $\alpha$ is the exponent for the inelastic cross-section, we find $\delta$=0.05 $\pm$0.08.

Within the framework of the Standard Model, the only known weakly interacting neutral particle is the neutrino. Hence, neutrino production may be expected to contribute some fraction of the observed missing energy tail. At our beam energy only semi-leptonic decay of charm can contribute significantly to $E_{mis} > 80$ GeV. Unfortunately, the experimental situation on charm production is confusing, if not bewildering [9, 10, 11]. This is illustrated in Figure 5, which shows the result of a Monte Carlo simulation of our beam dump configuration, using the Lund program [12, 13] as physics generator, but with different parametrisations of charm production according to the published results. Where necessary we have used $A^{0.75}$ [14] to extrapolate to different nuclei. The wide band in Figure 5 for $E_{mis} > 60$ GeV reflects the range of published data. Whilst the $A$ dependence of charm production is relevant here, it is in fact the shape of the $x_F$ spectrum which is crucial. Experiments which measure at lower $x_F$ tend to report a more steeply falling $x_F$ spectrum. On the other hand E613 [10] measure into the high $x_F$ region as we do, and they infer a much flatter $x_F$ spectrum. In Figure 6 we compare our data with the results of the Monte Carlo simulation using the E613 production spectra. The agreement is excellent for the heavy target data (beam dump), and acceptable, though slightly less good, for the light target data (target mode). It may be noted that the E613 production spectra come from their heavy target data, and their conclusions about any possible $A$ dependence of the $x_F$ spectrum are limited by statistics [14].

Whilst charm production is not the aim of the present analysis, it is clear that our data in the region $E_{mis} > 80$ GeV would support the E613 results in this region.

Upper limits on anomalous WINP production depend of course on what we take for the level of "background", i.e. charm. The most conservative approach is to take the lowest charm level implied by Figure 5. Since our data points lie well above such a level we can in practice set it to zero for the purposes of calculating upper limits. Assuming further a target atomic number dependence $A^{2/3}$ in order to extrapolate from pN to pp

collisions, Table 1 shows the 95% confidence level upper limits on the cross-section for non-interacting particles with energies above a certain threshold for the two configurations (target and beam dump). Alternatively we can take the charm level as measured by E613 to be the appropriate background level, and in this case we get the more restrictive upper limits given in Table 2.

| | $\geq 80$ | $\geq 100$ | $\geq 120$ |
|---|---|---|---|
| Target | - | $1.5 \times 10^{-5}$ | $6.2 \times 10^{-6}$ |
| Beam dump | $4.5 \times 10^{-5}$ | $2.0 \times 10^{-5}$ | $1.3 \times 10^{-5}$ |

Table 1: Cross-section limits (mbarns) for production of WINPs in pp collisions with energies above a certain threshold (GeV): no charm background.

| | $\geq 80$ | $\geq 100$ | $\geq 120$ |
|---|---|---|---|
| Target | - | $3.8 \times 10^{-6}$ | $2.0 \times 10^{-6}$ |
| Beam dump | $1.4 \times 10^{-5}$ | $5.4 \times 10^{-6}$ | $4.2 \times 10^{-6}$ |

Table 2: Cross-section limits (mbarns) for production of WINPs in pp collisions with energies above a certain threshold (GeV): charm background as measured by E613.

In order to extrapolate to the total cross-section for non-interacting particle production, WINPs of masses ranging from 0 to 5 GeV were then assumed to be produced according to the Bourquin-Gaillard formula [15]. In addition the dependence of the limits on the WINP life-time was studied to take into account the fact that the particles must traverse the calorimeters before decaying. Figure 7 shows the WINP production limits obtained at the 95% CL for different values of the life-time as a function of the particle mass. Also shown are the results adapted from [2].

## 5 Conclusion

A search for non-standard WINP production has been made using the missing energy technique. Limits on the production of new WINPs have been obtained for different masses and life-times; they represent an order of magnitude improvement on previous measurements.

**Acknowledgements**

The HELIOS collaboration wishes to thank the staff of the PS-SPS accelerator complex for their excellent work in providing the high quality proton beam used in this experiment. The valuable contributions of the technical staff of CERN and the collaborating institutes is gratefully acknowledged. We also wish to acknowledge the support received from the various research councils and funding agencies in our home countries.

## REFERENCES


[1] R. H. Bernstein et al., Phys. Rev. D 37 (1988) 3103 and references therein.
[2] J. P. Dishaw et al., Phys. Lett. B85 (1979) 142.
[3] R. Beuttenmuller et al., Nucl. Instr. and Methods A252 (1986) 471.
[4] T. Åkesson et al., HELIOS Collaboration, Zeit. Phys. C 38 (1988) 383.
[5] T. Åkesson et al., HELIOS Collaboration, Phys. Lett. B214 (1988) 295.
[6] T. Åkesson et al., Nucl. Instr. and Methods A262 (1987) 243.
[7] C. W. Fabjan, Proceedings of XXIVth International Conference on High Energy Physics, Munich, 1989.
[8] F. Gibrat, Thesis, Paris University, 1988.
[9] M. Aguilar-Benítez et al., Z. Phys. C 40 (1988) 321.
[10] M. E. Duffy et al., Phys. Rev. Lett. 57 (1986) 1522.
[11] J.L. Ritchie et al., Phys. Lett. 126B (1983) 499.
[12] G. Ingelman, Preprint DESY 86-131.
[13] B. Nilsson-Almqvist and E. Stenlund, LUNFD6 NFFK 7074-1-17-1986.
[14] M. E. Duffy et al., Phys. Rev. Lett. 55 (1985) 186.
[15] M. Bourquin and J.M. Gaillard, Nucl. Phys. B 114 (1976) 334.


## FIGURE CAPTIONS

**Fig. 1 :** The experimental layout, showing target region, calorimeters and downstream muon spectrometer.

**Fig. 2 :** Distribution of the Q variable ($Q = E_a/E_{vis}$) in different $E_{mis}$ bins. a) $0 < E_{mis} < 20$ GeV, b) $60 < E_{mis} < 80$ GeV, c) $80 < E_{mis} < 100$ GeV. The solid (dashed) line represents the distribution before (after) crack correction.

**Fig. 3 :** The beam dump missing energy spectrum as a function of squared beam rate $R^2$. Data for each of the 4 $E_{mis}$ bins has been divided into 3 rate bins. Also shown are the results of the fits in each bin.

**Fig. 4 :** Missing energy spectra for target and beam dump configurations. Points are data including systematic and statistical errors. The dashed lines correspond to the calorimeter resolution in each case.

**Fig. 5 :** Monte Carlo simulation of the beam dump missing energy spectrum using different charm parametrisations from published results.

**Fig. 6 :** Missing energy spectra for (a) beam dump and (b) target configurations. The histograms represent Monte Carlo results including classical sources of missing energy and using the E613 parametrisation of charm production.

**Fig. 7 :** Limits on the production of WINP particles as a function of mass for different life-times. Also shown are the limits obtained from [2].

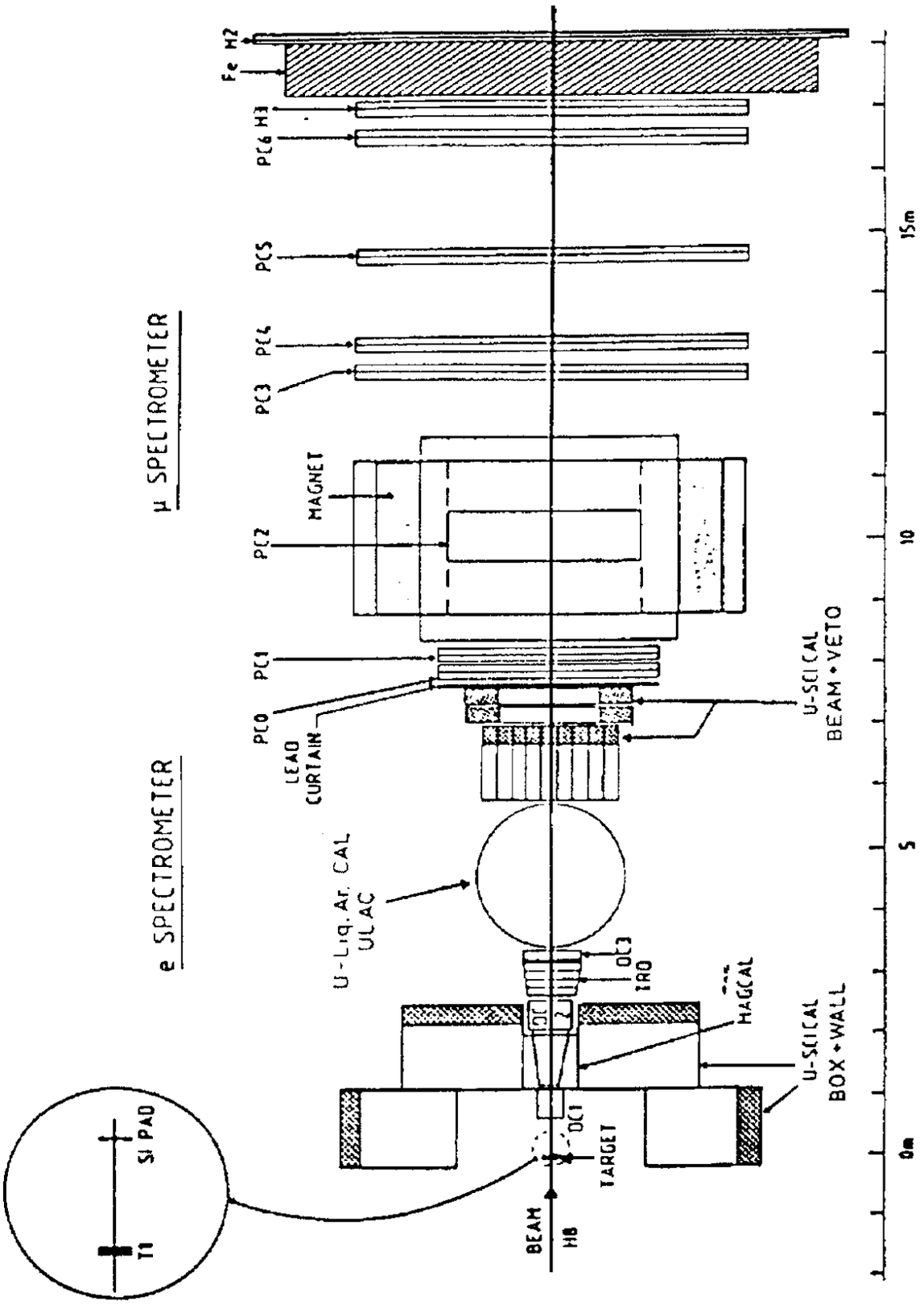
μ SPECTROMETER
e SPECTROMETER
Fe H2
PC6 H3
PC5
PC4
PC3
MAGNET
PC2
PC1
PC0
LEAD CURTAIN
U-SCICAL BEAM • VETO
U-Liq.Ar. CAL ULAC
DC3
TAO
HAGCAL
U-SCICAL BOX • WALL
DC1
TARGET
BEAM
H8
SI PAD
T1
0m
5
10
15m

Figure 1

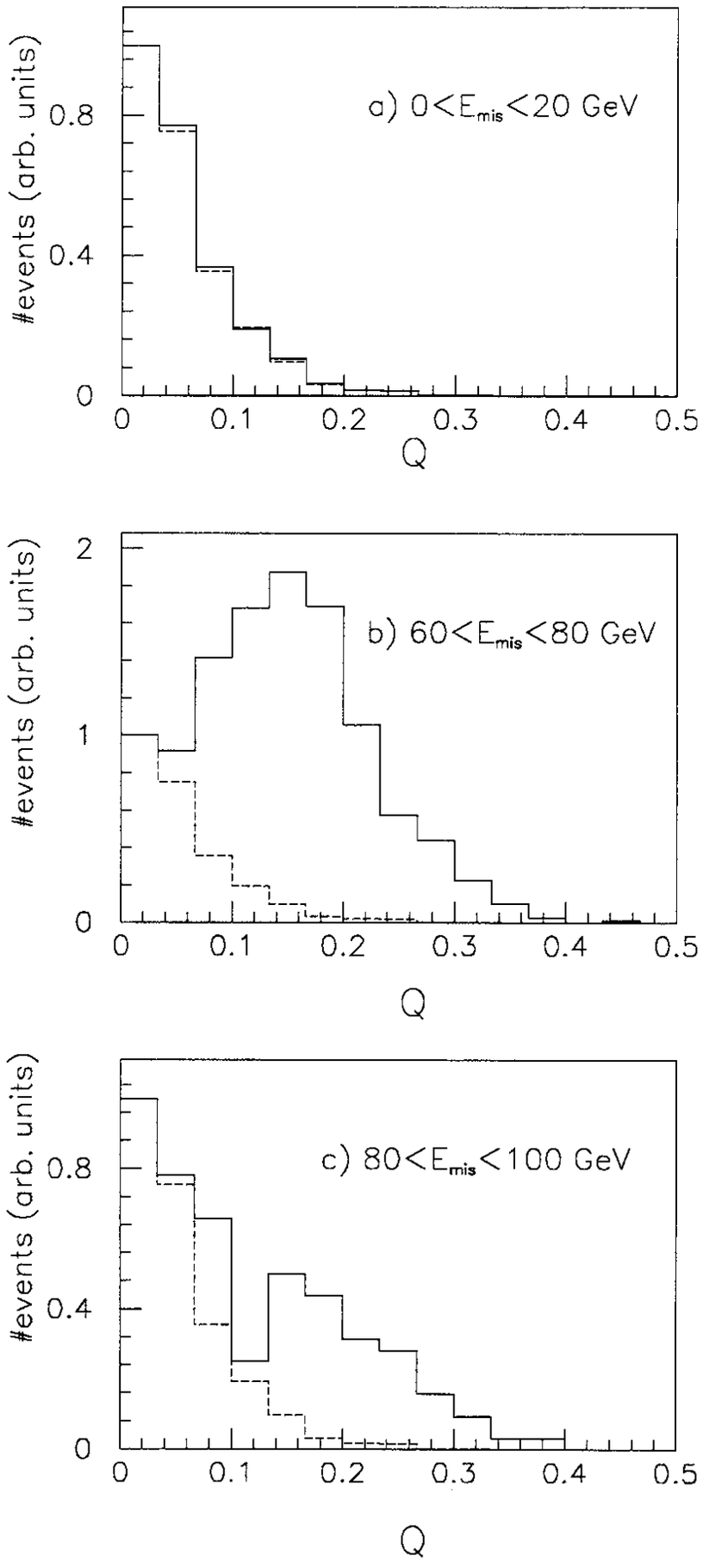
a) 0<E_mis<20 GeV
b) 60<E_mis<80 GeV
c) 80<E_mis<100 GeV
#events (arb. units)
Q
0
0.1
0.2
0.3
0.4
0.5
0.4
0.8
1
2

**Figure 2**

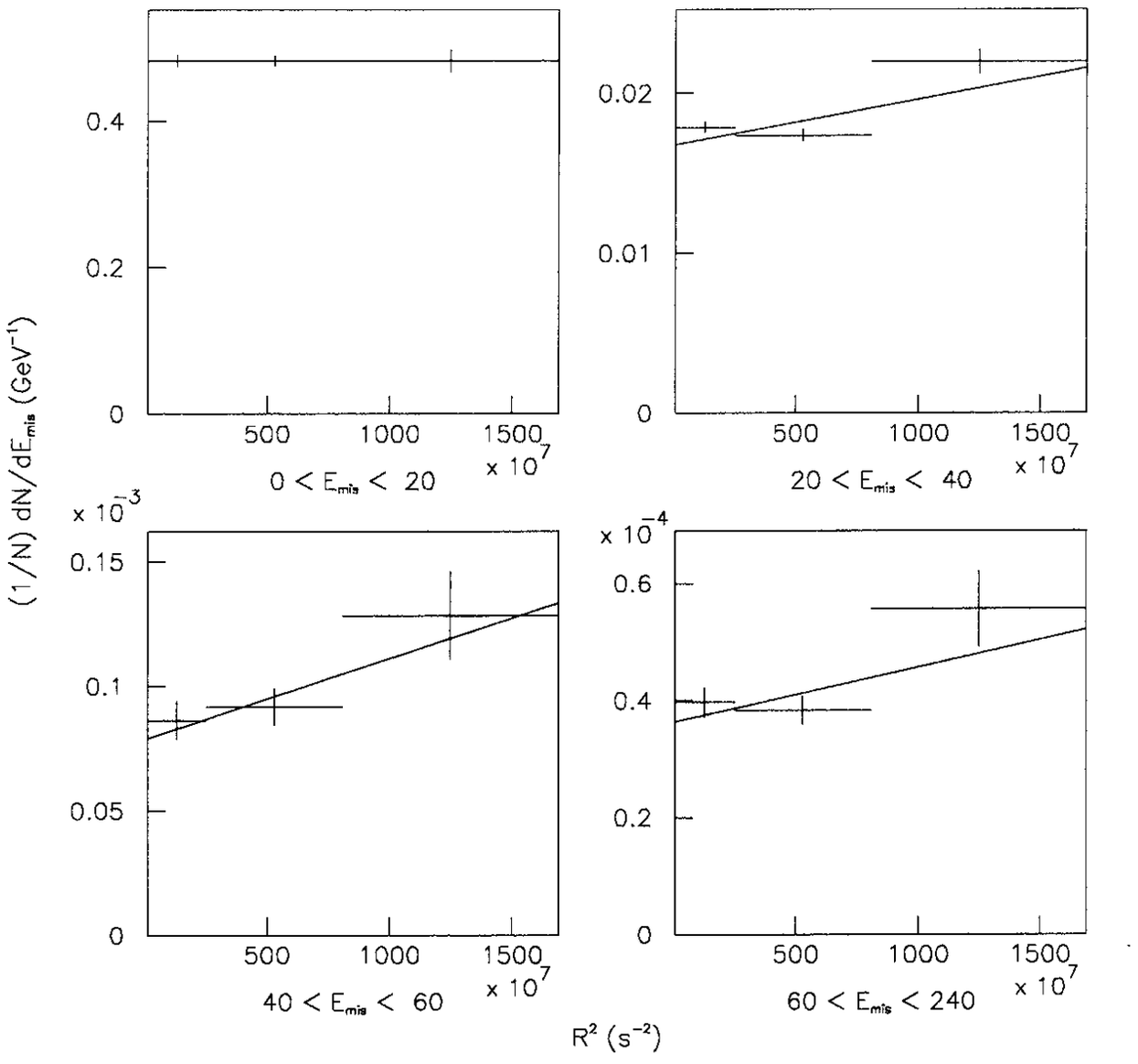
(1/N) dN/dE$_{mis}$ (GeV$^{-1}$)
0.4
0.2
0
500
1000
1500
x 10$^7$
0 < E$_{mis}$ < 20
0.02
0.01
0
500
1000
1500
x 10$^7$
20 < E$_{mis}$ < 40
x 10$^{-3}$
0.15
0.1
0.05
0
500
1000
1500
x 10$^7$
40 < E$_{mis}$ < 60
x 10$^{-4}$
0.6
0.4
0.2
0
500
1000
1500
x 10$^7$
60 < E$_{mis}$ < 240
R$^2$ (s$^{-2}$)

**Figure 3**

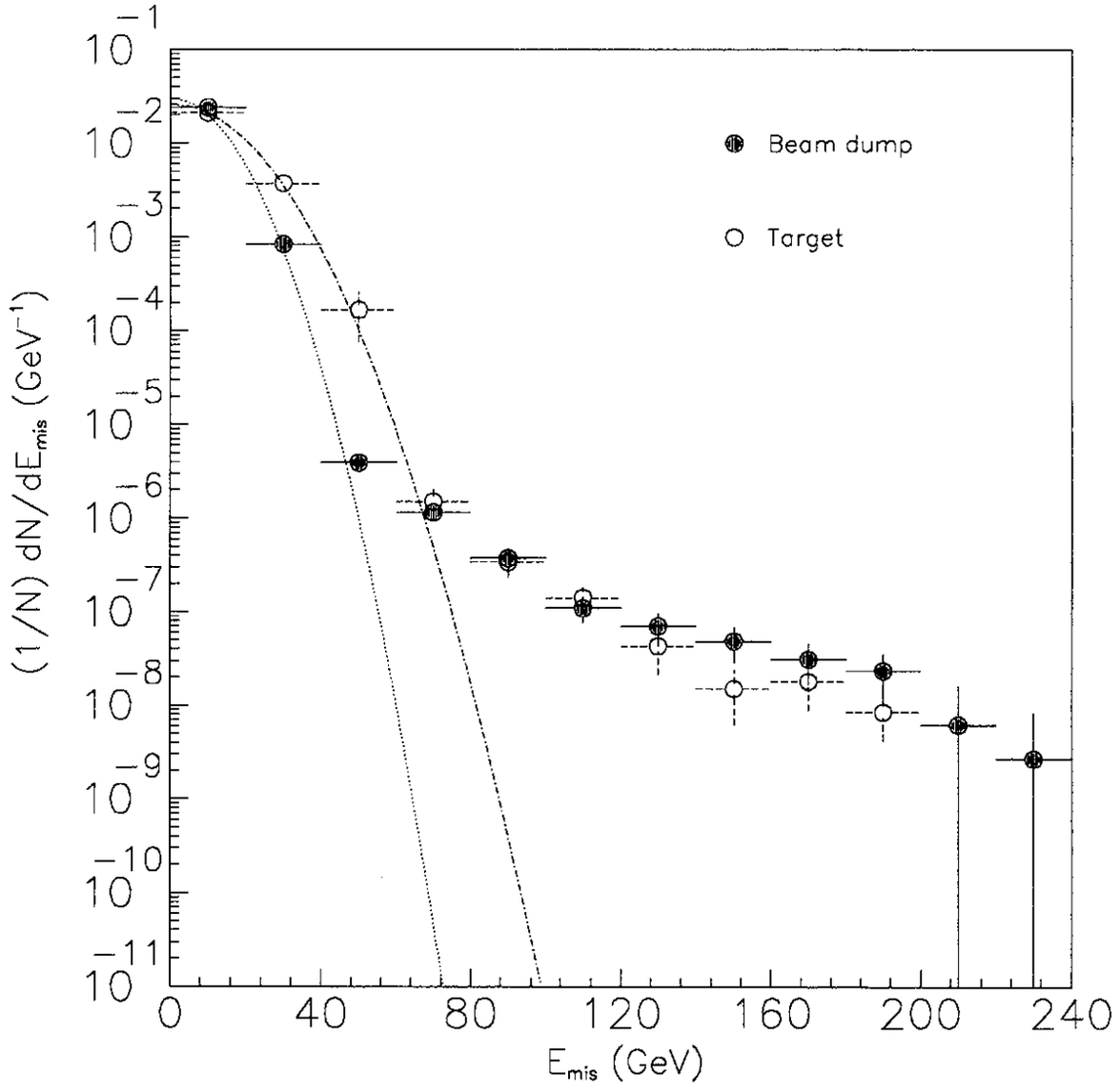
Beam dump
Target
(1/N) dN/dE$_{mis}$ (GeV$^{-1}$)
E$_{mis}$ (GeV)
10$^{-1}$
10$^{-2}$
10$^{-3}$
10$^{-4}$
10$^{-5}$
10$^{-6}$
10$^{-7}$
10$^{-8}$
10$^{-9}$
10$^{-10}$
10$^{-11}$
0
40
80
120
160
200
240

Figure 4

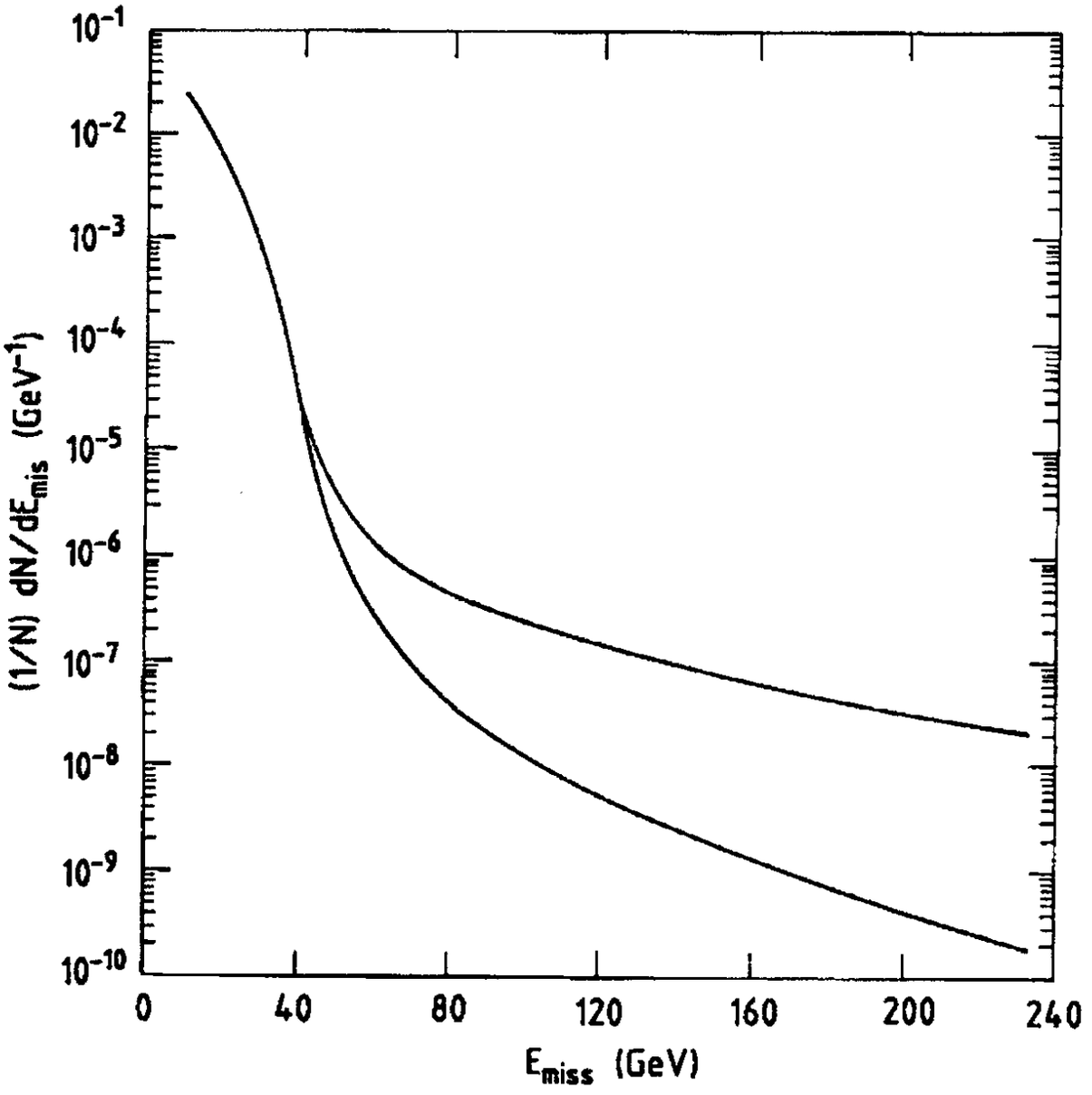
$10^{-1}$
$10^{-2}$
$10^{-3}$
$10^{-4}$
$10^{-5}$
$10^{-6}$
$10^{-7}$
$10^{-8}$
$10^{-9}$
$10^{-10}$
$(1/N)\ dN/dE_{mis}\ (GeV^{-1})$
0
40
80
120
160
200
240
$E_{miss}$ (GeV)

Figure 5

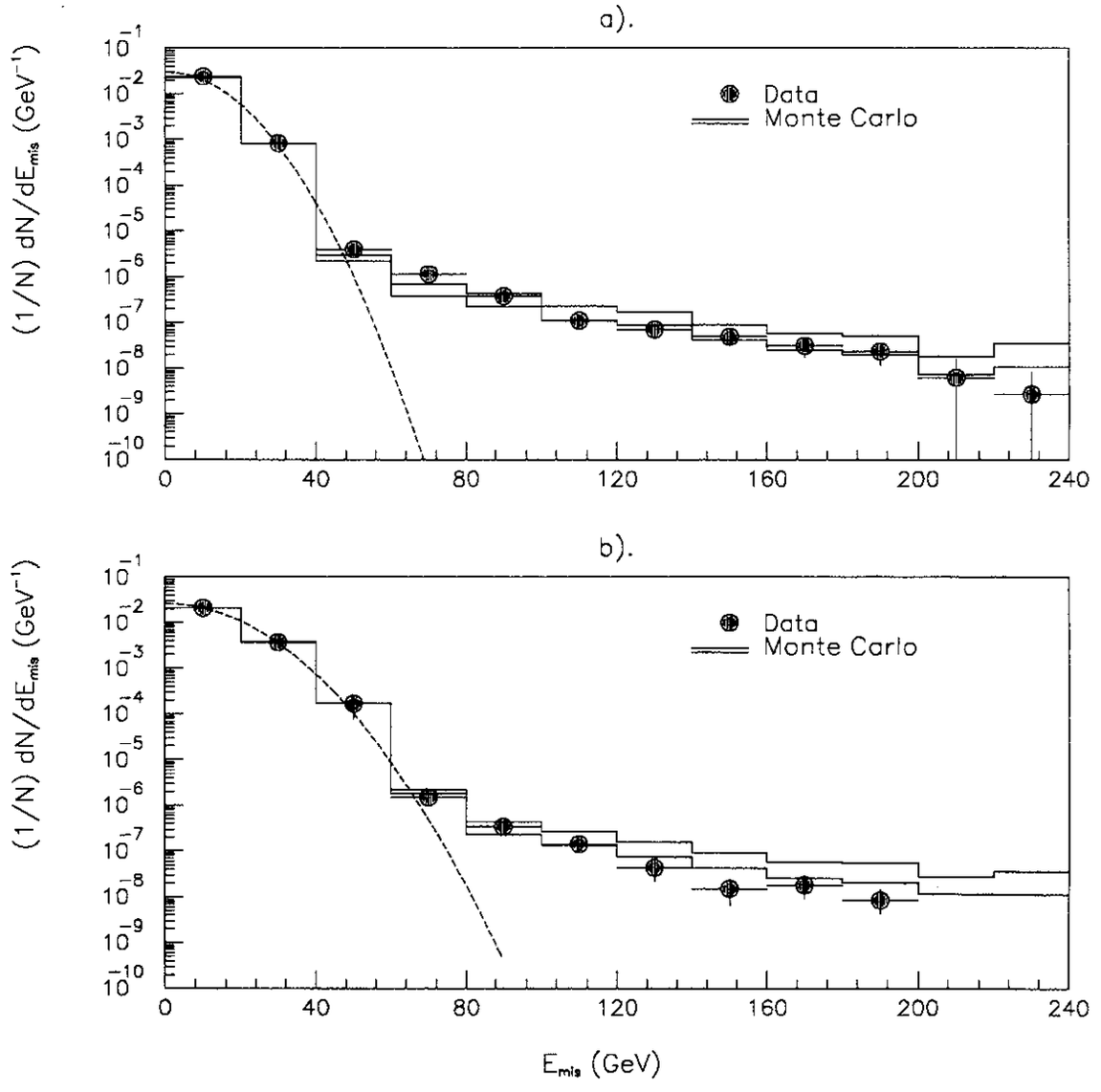
a).
b).
Data
Monte Carlo
(1/N) dN/dE$_{mis}$ (GeV$^{-1}$)
E$_{mis}$ (GeV)
0
40
80
120
160
200
240

Figure 6

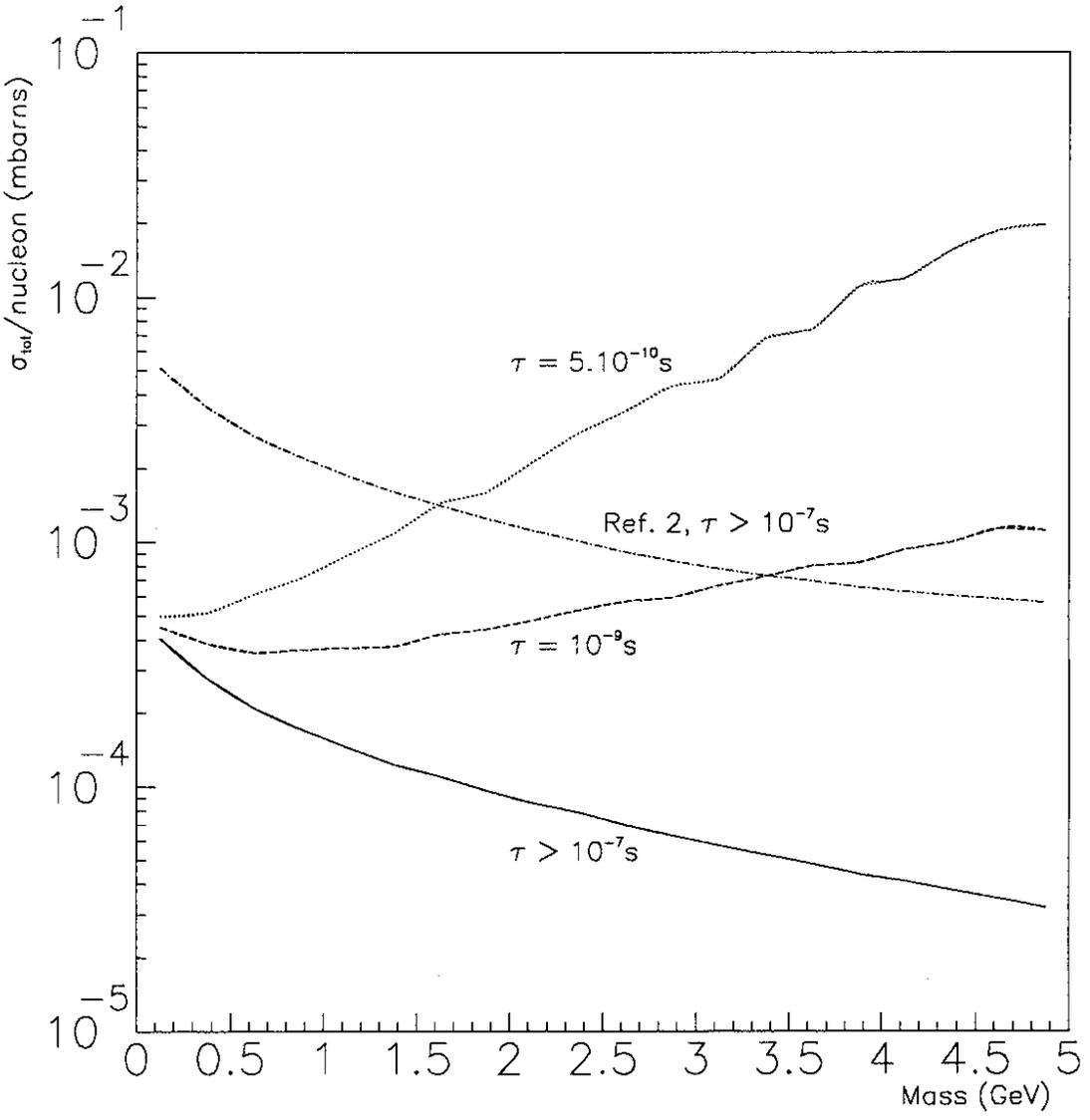
$\sigma_{tot}$/nucleon (mbarns)
$10^{-1}$
$10^{-2}$
$10^{-3}$
$10^{-4}$
$10^{-5}$
$\tau = 5.10^{-10}$s
Ref. 2, $\tau > 10^{-7}$s
$\tau = 10^{-9}$s
$\tau > 10^{-7}$s
0 0.5 1 1.5 2 2.5 3 3.5 4 4.5 5
Mass (GeV)

Figure 7